JCI insight

RESEARCH ARTICLE

Immunologic alterations in the pancreatic cancer microenvironment of patients treated with neoadjuvant chemotherapy and radiotherapy

Matthew R. Farren,[1] Layal Sayegh,[2] Michael Brandon Ware,[1] Hsiao-Rong Chen,[3] Jingjing Gong,[4] Yan Liang,[4] Alyssa Krasinskas,[5] Shishir K. Maithel,[6] Mohammad Zaidi,[6] Juan M. Sarmiento,[6] David Kooby,[6] Pretesh Patel,[7] Bassel El-Rayes,[1] Walid Shaib,[1] and Gregory B. Lesinski[1]

[1]Department of Hematology and Medical Oncology, Winship Cancer Institute, Emory University, Atlanta, Georgia, USA. [2]School of Medicine, Emory University, Atlanta, Georgia, USA. [3]Biostatistics and Bioinformatics Shared Resource, Winship Cancer Institute, Emory University, Atlanta, Georgia, USA. [4]Pathology Department, NanoString Inc., Seattle, Washington, USA. [5]Department of Pathology, [6]Department of Surgery, and [7]Department of Radiation Oncology, Winship Cancer Institute, Emory University, Atlanta, Georgia, USA.

Pancreatic ductal adenocarcinoma (PDAC) has dismal 5-year survival (<9%). We hypothesize that exposure of tumors to conventional therapies may preferentially modulate immune biomarkers in the tumor microenvironment in PDAC. PDAC patients who underwent upfront surgical resection or who received neoadjuvant FOLFIRINOX with or without neoadjuvant radiotherapy followed by surgical resection were selected for study. Total expression of immunologically relevant transcripts and spatially resolved expression of immunologically relevant proteins was quantitated using multiplexed methods (NanoString nCounter and GeoMX platforms). This analysis identified numerous differentially expressed transcripts associated with the type of neoadjuvant therapy received. Moreover, we identified significant alterations in the expression and/or spatial distribution of immunologically relevant proteins in different regions (tumor cell rich, immune cell rich, stromal cell rich) of the tumor microenvironment. These data provide insight into the immunological effects of clinically relevant neoadjuvant therapy for resectable/borderline-resectable PDAC by describing significant differences in the expression of key immunologic biomarkers within the PDAC microenvironment that were associated with the type of treatment patients received prior to surgical resection. This represents a comprehensive analysis of numerous biomarkers conducted on the PDAC microenvironment. This work may guide strategic new combination therapies for pancreatic cancer.

Conflict of interest: MRF received research and travel support from NanoString Inc. JG is an employee of NanoString Inc. YL is an employee of NanoString Inc. BE receives research support from several pharmaceutical companies (Boston Biomedical Inc., Bayer, Pfizer, Novartis, Merck, Bristol-Myers Squibb, and Roche) and consults for several companies (Astellas, Taiho, Ipsen, Novartis, Lexicon, and Roche). WS receives research support from Boston Biomedical Inc., Eli Lilly, and Lexicon and has received honoraria from Ipsen and Eisai. GBL has received compensation for consulting with ProDa Biotech LLC and has received research funding through sponsored research agreements between Emory University and Merck and Co. Inc., Boehringer Ingelheim Inc., Bristol-Myers Squibb Inc., and Vaccinex Inc.

Submitted: May 20, 2019
Accepted: December 4, 2019
Published: January 16, 2020.

Reference information: *JCI Insight*. 2020;5(1):e130362. https://doi.org/10.1172/jci.insight.130362.

Introduction

Pancreatic ductal adenocarcinoma (PDAC) is noted for its poor prognosis, with 5-year survival estimated at only 9% (1). The health effect of this disease continues to escalate, as recent studies indicate PDAC will be the second leading cause of cancer-related mortality by 2030 (2). Surgical resection remains a patient's best chance at curative therapy when tumors are detected early (3). However, even in successfully resected patients, prognosis remains grim, with median overall survival estimated as less than 23 months (4). As a result, surgical resection is often combined with chemotherapy and/or radiation therapy (3). While these conventional therapeutic modalities lead to modest improvement in overall survival, they are by no means curative in most individuals, emphasizing the need for improved therapeutic options.

PDAC tumors are unique by virtue of their histologic architecture (5). Notable factors include an abundant and fibrotic stroma, poor effector T cell infiltration, and diverse overlapping mechanisms of immune suppression (5). These complex cellular and fibrotic components of the tumor microenvironment pose a unique challenge to effective therapy, as they facilitate intricate interactions that limit drug penetration, fuel resistance, alter metabolic parameters, and drive resistance to immunotherapy (5). The mechanisms by which conventional treatment approaches, including chemotherapy and radiotherapy, affect the individual

cellular components of this tumor microenvironment in patients are poorly understood. In particular, uncovering how this chemotherapy and radiotherapy modulate signaling pathways and actionable immune targets in distinct tumor, stromal, or immune cell compartments could generate data to better inform the use of targeted or immune-based therapy following or in combination with chemotherapy and radiotherapy.

Immunotherapy continues to emerge as an alternative treatment approach in the setting of PDAC. Unfortunately, immunotherapeutic approaches targeting T cell immune checkpoints have not translated into efficacy against PDAC, despite their efficacy data in various other malignancies (6). This lack of efficacy may be related, in part, to the relatively low frequency of neoantigens in PDAC (6). However, the PDAC tumor microenvironment also contains several potentially immunosuppressive elements, particularly pancreatic stellate cells, as well as a dense stroma that may hinder the infiltration of tumor-reactive T cells and contribute to their exhausted phenotype (5, 6). Moreover, how the immune elements present within the PDAC tumor microenvironment are affected by conventional therapy regimens (chemotherapy, radiotherapy) is poorly defined. Indeed, there has been concern recently for how exposure to chemotherapy with or without radiation therapy may affect subsequent or concurrent immunotherapy approaches in PDAC. Potentially, conventional cytotoxic chemotherapy approaches could deplete or further impair tumor-reactive T cells, handicapping subsequent immunotherapies. An alternative scenario that is garnering much attention is whether chemotherapy or radiotherapy can be leveraged to elicit immunogenic cell death and reduction in immunosuppressive networks, thereby potentiating the response of PDAC to immunotherapy (6–8). Given that most PDAC patients receive chemotherapy and/or radiation therapy at some point during the course of their disease, understanding these interactions could be impactful across many patients and could influence subsequent response to any salvage treatment approaches.

We hypothesized that neoadjuvant FOLFIRINOX (a combination of fluorouracil, folinic acid, irinotecan, and oxaliplatin) (3) alone or combined with radiotherapy will preferentially modulate immune biomarkers in the tumor microenvironment of PDAC. In this report, we captured gene expression profiles and used multiplex GeoMx analysis of distinct spatial compartments to compare patient PDAC tumors exposed to FOLFIRINOX, with or without radiotherapy, to those resected without any neoadjuvant therapy. Several actionable signaling and immune biomarkers were identified in tumor, stroma, and immune cell compartments of PDAC tumors that may inform how conventional therapy can be maneuvered for improved efficacy.

Results

Patient characteristics. We obtained archival tissue from 24 patients who received surgical resection of PDAC tumors at Emory University (Table 1). Six patients had received no treatment for their cancer prior to surgery (surgery alone), six patients received neoadjuvant FOLFIRINOX prior to surgery (FOLFIRINOX), six patients received neoadjuvant FOLFIRINOX followed by stereotactic body radiotherapy (SBRT) (F + SBRT) prior to surgery, and six patients received neoadjuvant FOLFIRINOX followed by conventional (nonstereotactic) radiotherapy (F + XRT) prior to surgery. In all cases, radiotherapy followed the completion of chemotherapy. The number of cycles of chemotherapy that patients received was variable but ranged between 1.5 and 3 cycles (Table 1). Likewise, the elapsed time between diagnosis, the end of chemotherapy, or the end of radiotherapy and surgical resection is detailed in Table 1, by group. Long-term follow-up of patient outcome was not available for 13 of 24 patients due to missing data for many individuals who were referred to our center from the community.

Combination chemotherapy and radiotherapy is associated with long-term alterations in the abundance of immunologically relevant transcripts within PDAC tumors. To assess the effect of neoadjuvant therapy on gene expression patterns related to immunologic function in PDAC tumors, transcript levels of 770 predefined immunologically relevant genes from surgically resected, formalin-fixed, paraffin-preserved (FFPE) pancreatic adenocarcinomas were assessed using the NanoString nCounter platform (Figure 1A). Among all groups, a total of 189 differentially expressed genes (DEGs) were identified (Figure 1B and Supplemental Table 2; supplemental material available online with this article; https://doi.org/10.1172/jci.insight.130362DS1). There were no DEGs between surgery-alone patients and those treated with FOLFIRINOX after adjusting for FDR (adjusted $P < 0.05$, Figure 1C). Compared with tumors from surgery-alone patients, tumors from patients who received F + SBRT exhibited 132 DEGs, 110 with higher expression and 22 with lower expression (Figure 1D). 105 DEGs had higher expression in F + XRT–treated tumors and 16 had lower expression in comparison with surgery-alone patient tumors (Figure 1E). We carried out a similar set of analyses, comparing gene expression in F + SBRT– and F + XRT–treated tumors with FOLFIRINOX-treated tumors.

Table 1. Patient characteristics

Neoadjuvant therapy	None (*n* = 6)	FOLFIRINOX (*n* = 6)	FOLFIRINOX + SBRT (*n* = 6)	FOLFIRINOX + XRT (*n* = 6)
Age at diagnosis (yr)				
Mean	62.8	62.0	62.3	62.0
Range	44–77	49–76	49–76	49–68
Sex				
Female	0	3	4	4
Male	6	3	2	2
Race				
African American	1	1	0	2
White	4	5	5	4
All others	1	0	1	0
Tumor location				
Head	5	5	6	4
Body	0	0	0	0
Neck	0	1	0	0
Tail	1	0	0	2
Initial stage				
Resectable	6	1	0	0
Borderline resectable	0	5	6	4
Locally advanced	0	0	0	2
Differentiation				
Well	0	1	0	1
Moderate	4	3	5	4
Poor	2	2	1	1
Lymphovascular invasion				
No	5	4	5	5
Yes	1	2	1	1
Perineural invasion				
No	6	6	5	6
Yes	0	0	1	0
Cycles of FOLFIRINOX				
Mean	n/a	1.83	2.00	2.30
Range	n/a	1.5–2.0	All received 2 cycles	1.5–3.0
Time from diagnosis to surgery (wk)				
Mean	9.5	17.1	19.9	29.9
Range	2.3–40.4	11.3–20.6	18.3–22.1	23.4–35.0
Time from end of neoadjuvant therapy to surgery (wk)				
Mean	n/a	6.6	9.4	17.0
Range	n/a	2.9–11.4	7.4–11.0	16.1–18.3

When comparing FOLFIRINOX-treated tumors with F + SBRT–treated tumors, there were 40 DEGs expressed at higher levels in F + SBRT–treated tumors and 10 with higher expression in FOLFIRINOX-treated tumors (Figure 1F). Comparing F + XRT– with FOLFIRINOX-treated tumors, 73 DEGs were expressed at higher levels in F + XRT–treated tumors and 10 were expressed at lower levels (Figure 1G). There were no DEGs when comparing patients treated with F + SBRT to those treated with F + XRT (data not shown). Among the DEGs observed in multiple groups, all of them were differentially expressed in the same direction in their respective groups (i.e., no DEGs were expressed at a higher level in F + SBRT–treated tumors compared with surgery-alone tumors or FOLFIRINOX-treated tumors or were expressed at a lower level in F + XRT–treated tumors compared with surgery-alone or FOLFIRINOX-treated tumors).

Bioinformatic analyses identify gene sets and protein networks associated with prior FOLFIRINOX plus radiation therapy exposure. Gene set enrichment analysis was used to identify the top-ranked upregulated (more highly expressed in FOLFIRINOX plus radiotherapy) and downregulated (more highly expressed in surgery alone of FOLFIRINOX alone) gene sets/pathways/processes in each combination treatment condition,

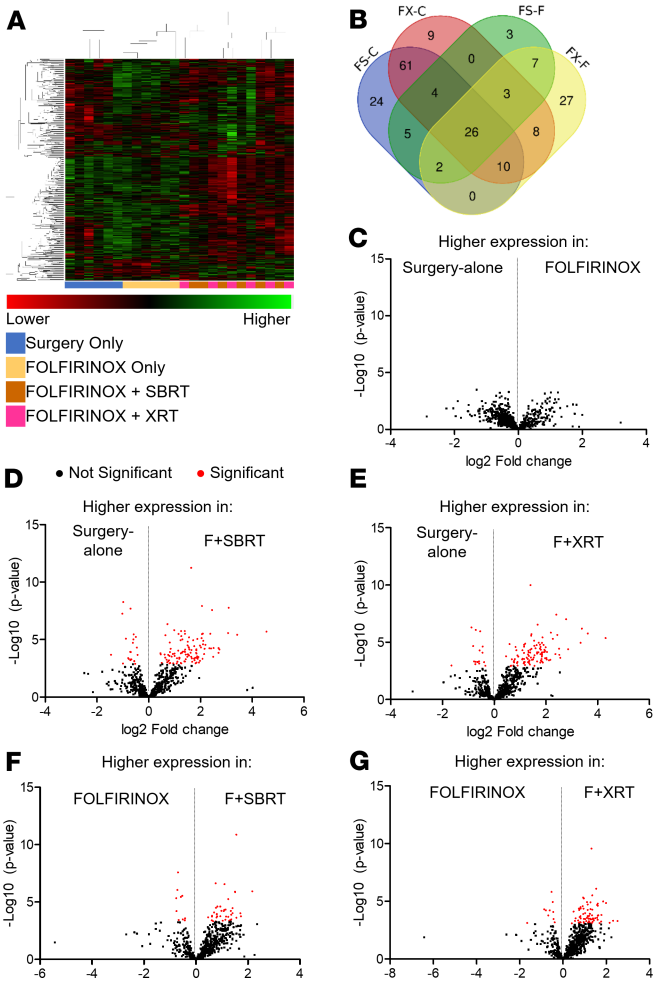

Figure 1. Neoadjuvant FOLFIRINOX plus radiotherapy is associated with substantial alterations in immunologically relevant gene expression. (**A**) Heat map clustering of gene expression in archival PDAC samples resected from patients who received no neoadjuvant therapy, neoadjuvant FOLFIRINOX, or neoadjuvant FOLFIRINOX plus stereotactic beam radiotherapy or external beam radiotherapy (n = 6 patients/treatment group). Each column represents 1 individual patient tumor, and each row represents 1 gene. Unsupervised hierarchical clustering of genes and samples was carried out by uncentered Pearson correlation. Color indicates normalized counts of each gene, with red representing higher expression and green relatively lower expression. (**B**) Venn diagram indicating how many differentially expressed genes were found in each comparison and how many genes overlapped each set of comparisons. FS-C, F + SBRT versus surgery alone; FX-C, F + XRT versus surgery alone; FS-F, F + SBRT versus FOLFIRINOX; FX-F, F + XRT versus FOLFIRINOX. (**C**–**G**) Volcano plots depicting differentially expressed gene P value as a function of fold change between the indicated groups. Red dots indicate FDR-adjusted P value of less than 0.05. (**C**) DEGs in FOLFIRINOX-treated vs. surgery-alone tumors. (**D**) DEGs in F + SBRT–treated vs. surgery-alone tumors. (**E**) DEGs in F + XRT–treated vs. surgery-alone tumors. (**F**) DEGs in F + SBRT–treated versus FOLFIRINOX-treated tumors. (**G**) DEGs in F + XRT–treated versus FOLFIRINOX-treated tumors.

compared with surgery-alone and FOLFIRINOX (Supplemental Table 3). Since the assay used to quantify changes in gene expression was composed primarily of immunologically relevant genes, it is not surprising that immune gene sets dominate the top-ranked increased and decreased expression (compared with surgery only or FOLFIRINOX) gene sets in this analysis. To further elucidate the potential biological effect of these DEGs, we also analyzed the data using protein-protein interaction enrichment analysis and the Molecular Complex Detection (MCODE) algorithm (6). These results identified a diverse and interconnected network of immune genes that are enriched in PDAC tumors exposed to FOLFIRINOX plus radiotherapy, including interferon-related transcripts, cytokine and NF-κB–related transcripts, and complement cascade related transcripts as well as greater levels of CD8a, CD8b, costimulatory, and checkpoint molecules (Supplemental Figures 2–5). These data identify a number of potential molecular mediators of the immunological response to chemotherapy/radiotherapy.

To better understand the genetic networks being induced or repressed by FOLFIRINOX plus radiotherapy, we analyzed the promoters of the DEGs identified above using EnrichR (TRANSFAC and JASPAR PWMs) to identify transcription factor–binding motifs that were enriched within the data set (9–11). This analysis identified a total of 48 transcription factors whose target motifs were statistically enriched (FDR-adjusted $P < 0.05$) in the DEGs: 47 within the data sets of upregulated DEGs and 1 (SRF) within the data sets of downregulated DEG (Supplemental Tables 4–7). Target motifs for 2 of these transcription factors, RUNX1 and SND1, were significantly enriched in all 4 comparison groups (F + SBRT versus surgery alone, F + XRT versus surgery alone, F + SBRT versus FOLFIRINOX, F + XRT versus FOLFIRINOX). This analysis suggests that RUNX1 and SND1 may be major mediators of any immunological response to chemotherapy/radiotherapy in PDAC.

Neoadjuvant therapy with FOLFIRINOX with or without stereotactic radiation is associated with durable, profound differences in the PDAC tumor microenvironment. Changes in the quantity and spatial distribution

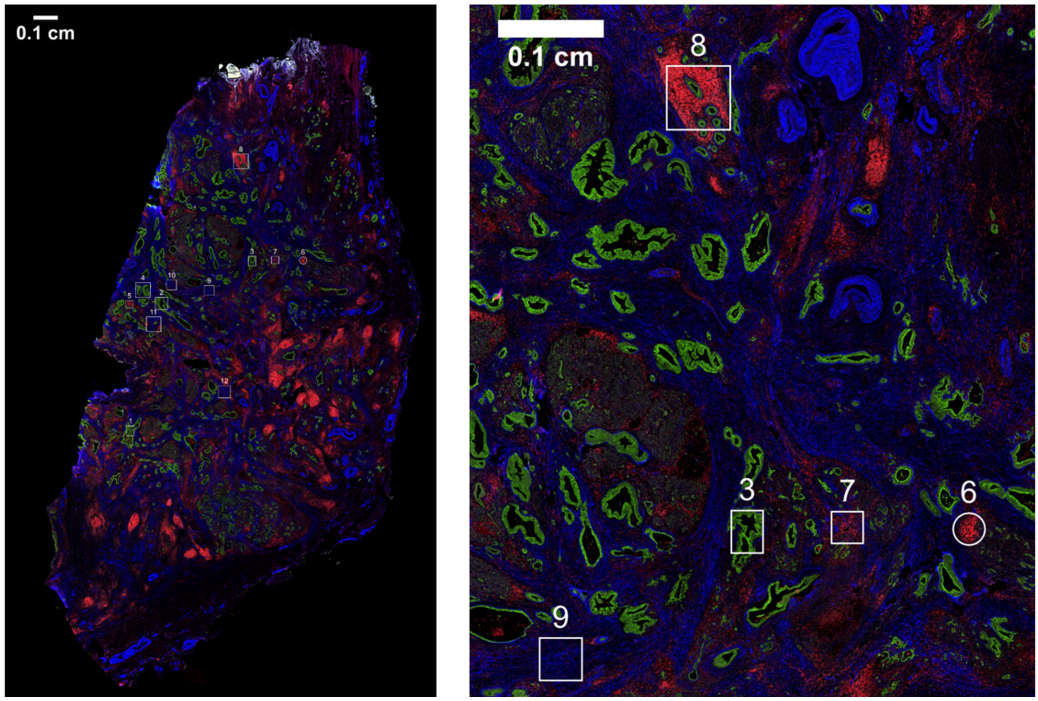

Figure 2. Selection of tumor-rich, immune cell–rich, and stroma-rich regions within PDAC tumors. As part of GeoMX workflow, FFPE slides of PDAC tumors from patients who received upfront surgical resection or surgical resection following neoadjuvant therapy with either FOLFIRINOX alone or FOLFIRINOX + SBRT were stained with fluorescently labeled anti–pan-cytokeratin (green), anti-CD45 (red), and anti–α-smooth muscle actin (αSMA, blue). A representative slide is shown. These fluorescently labeled antibodies were used to manually define regions of interest with the intent being to select tumor-rich regions (rich in pan-cytokeratin staining but largely lacking CD45 and αSMA staining), immune cell–rich regions (rich in CD45 staining but largely lacking pan-cytokeratin and αSMA staining), and stroma-rich regions (rich in αSMA but largely lacking the other 2 markers). Scale bar: 0.1 cm.

of various immune-related protein markers in the PDAC tumor microenvironment were next assessed using the GeoMX platform (NanoString Inc.). This platform measures protein abundance in a multiplexed and spatially resolved manner. We selected 12 target regions per PDAC tumor on the basis of fluorescently labeled anti-CD45, anti–pan-cytokeratin, and anti–α-smooth muscle actin (αSMA), which were used essentially to "map" the tissue (Figure 2 and Supplemental Figure 1). Based on these fluorescent labels, we selected "immune cell–rich" regions that were enriched for CD45 staining, "tumor-rich" regions that were enriched for pan-cytokeratin, and "stroma-rich" regions that were enriched for αSMA and lacked large amounts of CD45 or pan-cytokeratin staining (Figure 2 and Supplemental Figure 1). To the extent that was possible, these regions were selected in such a way that CD45-rich regions contained a minimal amount of pan-cytokeratin and αSMA staining, that tumor-rich regions contained a minimal amount of CD45 and αSMA staining, and that stroma-rich regions contained a minimal amount of pan-cytokeratin and CD45 staining. Though we intended to select and analyze 4 regions of each type from every surgery-alone, FOLFIRINOX-treated, and F + SBRT–treated tumor (n = 6 each), some regions were lost for technical reasons, resulting in a final analysis of 71 tumor-rich regions (24 surgery alone, 23 FOLFIRINOX, 24 F + SBRT), 70 immune-rich regions (24 surgery alone, 24 FOLFIRINOX, 22 F + SBRT), and 69 stroma-rich regions (22 surgery alone, 24 FOLFIRINOX, 23 F + SBRT). Descriptive statistics for each tissue type are included in Supplemental Table 8.

Within pan-cytokeratin–rich regions, neoadjuvant therapy is associated with alterations in signaling pathways, cell survival pathways, and VISTA expression. Within the tumor-rich regions, the abundance of 11 proteins differed significantly among the treatment groups. Neoadjuvant therapy was associated with alterations in several signaling pathways within tumor-rich regions (Figure 3A). F + SBRT, but not FOLFIRINOX, was associated with decreased AKT, β-catenin, and STAT3 expression (Figure 3A) when compared with surgery-alone patients. Note that while total levels of AKT and STAT3 differed among the patient groups, the amount of the phosphorylated proteins (i.e., the active signaling form of the molecules) did

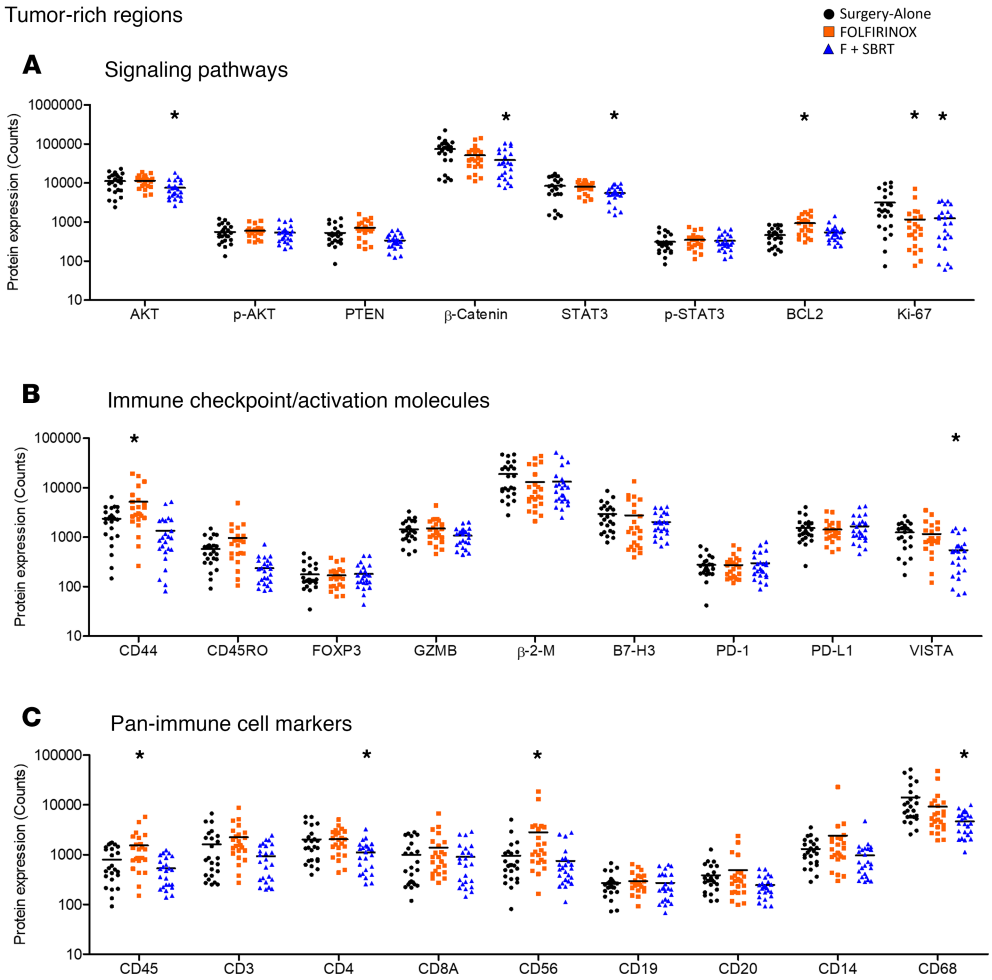

Figure 3. Neoadjuvant therapy alters the expression levels of immunologically relevant proteins in tumor-rich regions. Expression levels of the indicated proteins. Each dot represents a single region of interest. Individual regions of interest were derived from each patient tumor from a total of $n = 6$ patient tumors. (**A**) Signaling pathways. Expression level of signal transduction molecules and cell-cycle–related proteins within tumor-rich regions. (**B**) Immune checkpoint/activating molecules. Expression level of T cell checkpoint molecules, effector molecules, and other proteins that indicate immune cell phenotype within tumor-rich regions. (**C**) Pan-immune cell markers. Expression level of proteins that indicate immune cell type within tumor-rich regions. *FDR < 0.05 by 1-way ANOVA followed by post test in comparison to surgery-alone patients.

not differ significantly (Figure 3A). Ki67, a marker of proliferating cells, was lower within tumor regions that received either neoadjuvant therapy (F and F + SBRT) compared with that in tumors from patients who had surgery alone (Figure 3A). Neoadjuvant FOLFIRINOX was further associated with significantly higher BCL2 expression within tumor-rich regions compared with surgery-alone tumors, though this was not evident when patients also received SBRT (Figure 3A).

Expression levels of T cell checkpoint molecules and other immunologically relevant proteins in these tumor-rich regions also differed among patients in the different treatment groups. CD44, a molecule that — among other things — is expressed on activated T cells (12, 13), was present at higher levels in FOLFIRINOX-treated patients than in surgery-alone patients (Figure 3B). VISTA, an immunosuppressive checkpoint molecule (14), was expressed at significantly lower levels in F + SBRT–treated patients than in surgery-alone patients (Figure 3B). Neoadjuvant therapy was also associated with significant differences in the amount of CD45 and several proteins that serve as markers of immune cell type (CD4, CD45, CD56, CD68; Figure 3C). However, it must be noted that the absolute amount of CD45 and CD4 in the tumor-rich regions was present at a substantially lower level than in the immune-rich regions based on our selection strategy (on the order of ≤10%–15%) (Figure 3C, Figure 4A, and data not shown).

FOLFIRINOX is associated with higher levels of granzyme B and PD-L1 within CD45-rich regions, while F + SBRT is associated with lower levels of T cell markers and markers of antigen-experienced T cells. Neoadjuvant therapy was associated with substantial alterations within immune cell–rich regions of PDAC tumors, with the expression of 16 proteins differing significantly between groups. Interestingly, the abundance of the CD3, CD4, and CD8a T cell markers was not significantly different in hematopoietic-rich regions from surgery-alone and FOLFIRINOX-treated patients (Figure 4A). CD3 and CD4, however, were significantly lower in F + SBRT–treated patients (Figure 4C), as were CD44 and CD45RO (Figure 4B). Neoadjuvant therapy was also associated with significant differences in the expression of the B cell markers CD19 and CD20 and of the monocyte marker CD14 (Figure 4C). Patients who received F + SBRT also expressed significantly lower levels of the PD-1 and VISTA checkpoint molecules than did surgery-alone patients (Figure 4B). In contrast FOLFIRINOX neoadjuvant therapy was associated with significantly higher levels of granzyme B and PD-1 compared with surgery alone.

As observed in tumor-rich regions, neoadjuvant therapy was also associated with differences in signaling pathways within immune cell–rich regions (Figure 4C). Notable differences between groups were evident in pathways, including pSTAT3, PTEN, and BCL2, that regulate metastasis, survival, and other cellular functions.

Within stroma-rich regions, differences in signaling and checkpoint molecules were associated with neoadjuvant therapy. Within the stroma-rich regions, there were 19 proteins whose expression differed significantly among the treatment groups. Consistent with that observed in tumor-rich and hematopoietic-rich regions, neoadjuvant therapy was associated with significant differences in proteins associated with cell survival, proliferation, and signal transduction, specifically PTEN, β-catenin, BCL2, and Ki-67 (Figure 5A). Moreover, the expression levels of the checkpoint molecules PD-1 and VISTA also differed significantly among patients in the different treatment groups (Figure 5B). It was unclear what cellular source within these stroma-rich regions accounted for these differences in PD-1 and VISTA expression, as antibodies targeting these proteins were not fluorochrome conjugated. Neoadjuvant F + SBRT was also associated with significant differences in the expression level of several other proteins with a role in immune cell function, or that denote activation/maturation status, as compared with surgery-alone patients (Figure 5B).

Neoadjuvant therapy was also associated with significant differences in the amount of many pan-immune cell markers detected within stroma-rich regions (CD45, CD3, CD4, CD8A, CD19, CD20, CD56, CD68; Figure 5C.). As with tumor-rich regions, however, it should be noted that the absolute amount of CD45 and most of the other pan-immune cell markers was present at a substantially lower level than in the immune-rich regions (Figure 5C and Figure 4A).

Discussion

Pancreatic cancer, despite marginal improvements in survival over the last several years, continues to have a very poor prognosis and is generally unresponsive to therapy. This resistance to therapeutic approaches extends to immunotherapy, with very few patients responding to immune checkpoint blockade. In this report, we examined the effects that 1 type of conventional standard of care therapy (FOLFIRINOX, with/without 2 types of radiotherapy) has on immune biomarkers within the tumor microenvironment.

These results directly identify upregulated and downregulated genes within the tumor microenvironment following neoadjuvant therapy, when compared with patients who received surgical resection without neoadjuvant therapy. Alterations in gene expression induced by these neoadjuvant therapies were sufficiently durable that unsupervised hierarchical clustering of the resulting gene expression profiling data distinguished tumors from patients who received upfront surgical resection from those who received neoadjuvant therapy (FOLFIRINOX alone or FOLFIRINOX plus radiotherapy), even weeks to months afterword. These gene expression profiling analyses identified several immunologically relevant gene families/networks that are induced by neoadjuvant FOLFIRINOX plus radiotherapy, including interferon-family genes, complement-cascade genes, and signal transduction pathways involved in inflammation or immune responses. These observations argue that these therapies are associated with differential modulation of immune-related genes and there may be opportunity to leverage these changes to potentiate immunotherapy.

As part of this study, bioinformatic analyses were carried out, assessing the presence or absence of various transcription factor–binding sites within the promoters of differentially expressed genes. This analysis found that the binding site motifs for the transcription factors RUNX1 and SND1 were significantly

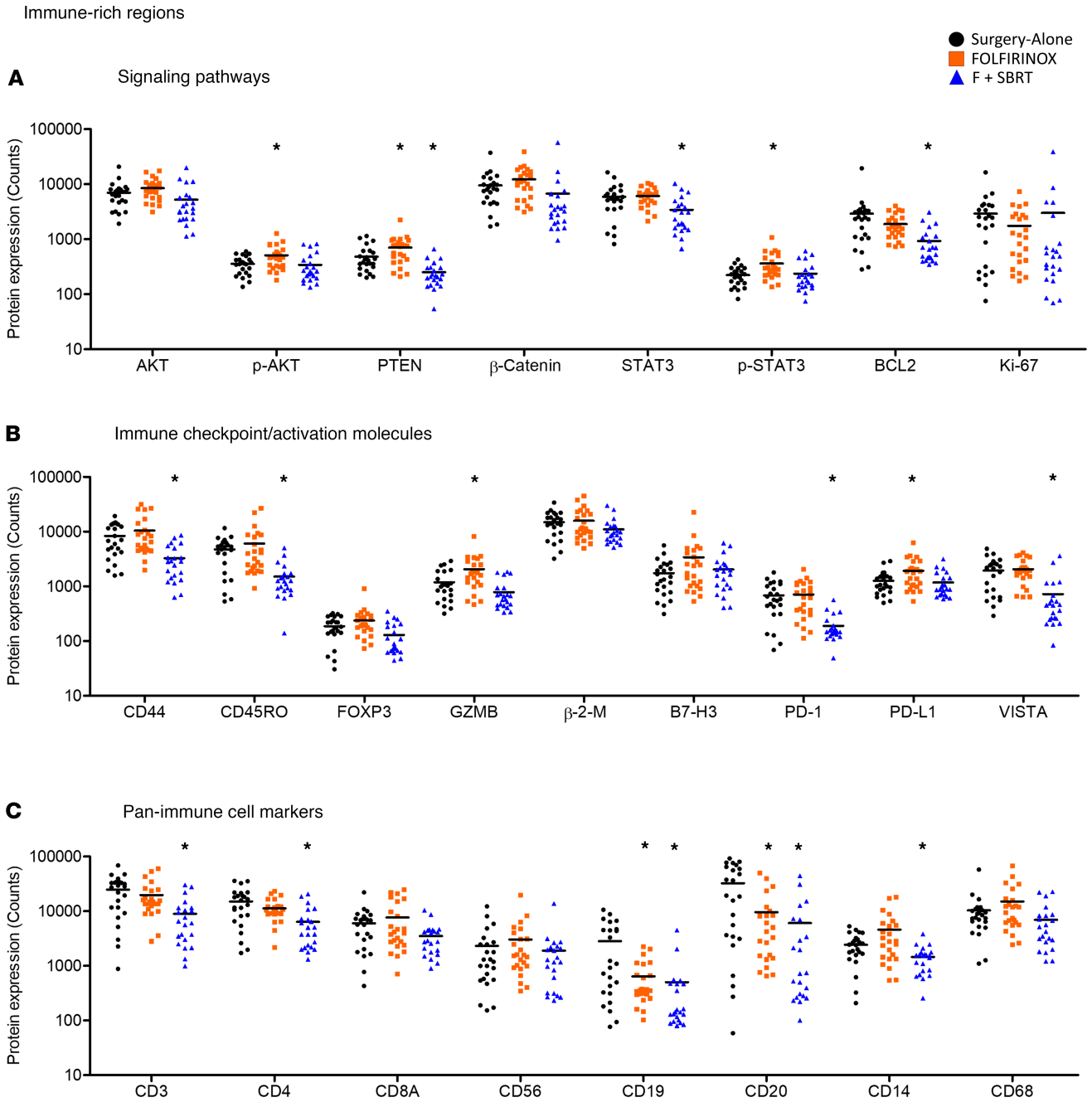

Figure 4. Neoadjuvant therapy alters the expression levels of immunologically relevant proteins in immune cell–rich regions. Expression levels of the indicated proteins. Each dot represents a single region of interest. Individual regions of interest were derived from each patient tumor from a total of $n = 6$ patient tumors. (**A**) Signaling pathways. Expression level of signal transduction molecules and cell-cycle–related proteins within immune cell–rich regions. **FDR < 0.05 by 1-way ANOVA followed by post test in comparison to surgery-alone patients. (**B**) Immune checkpoint/activating molecules. Expression level of T cell checkpoint molecules, effector molecules, and other proteins that indicate immune cell phenotype within immune cell–rich regions. (**C**) Pan-immune cell markers. Expression level of proteins that indicate immune cell type within immune cell–rich regions.

enriched among genes that were more highly expressed when F + SBRT– or F + XRT–treated tumors were compared with surgery-alone or FOLFIRINOX-treated tumors. RUNX1 is a transcription factor with prominent functions in hematopoiesis, among other cellular processes (15). While it has been studied in solid malignancies, both as a tumor suppressor and as an oncogene, it has received very little attention in pancreatic cancer (15). One report found high levels of RUNX1 expression in PDAC and argued that it increased the aggressiveness of PDAC cells by suppressing mIR-93 (16). Even less has been reported about the potentially oncogenic (17) transcription factor SND1 in pancreatic cancer, and we could find no

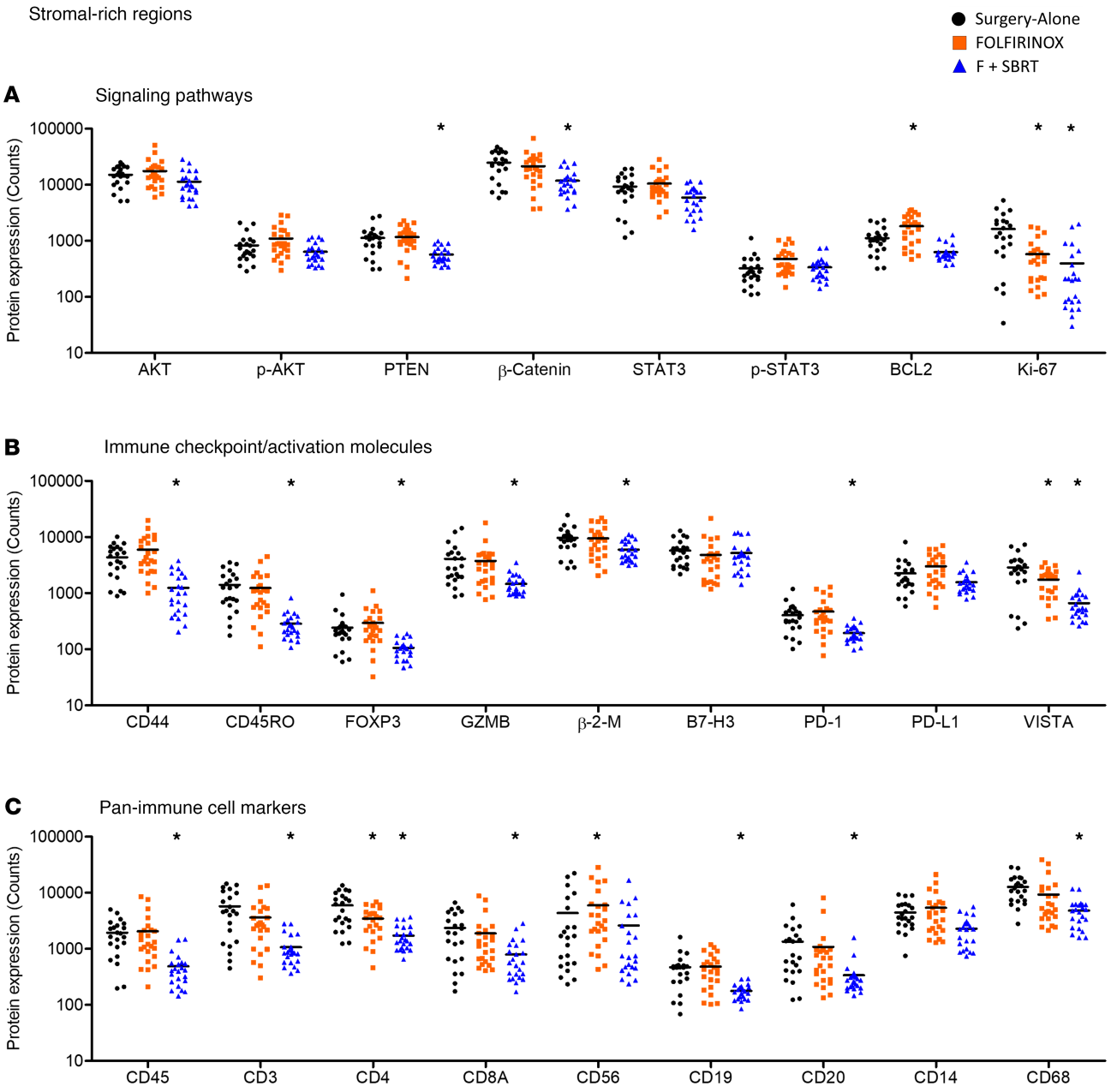

Figure 5. Neoadjuvant therapy alters the expression levels of immunologically relevant proteins in stroma-rich regions. Expression levels of the indicated proteins. Each dot represents a single region of interest. Individual regions of interest were derived from each patient tumor from a total of $n = 6$ patient tumors. (**A**) Signaling pathways. Expression level of signal transduction molecules and cell-cycle–related proteins within stroma-rich regions. (**B**) Immune checkpoint/activating molecules. Expression level of T cell checkpoint molecules, effector molecules, and other proteins that indicate immune cell phenotype within stroma-rich regions. (**C**) Pan-immune cell markers. Expression level of proteins that indicate immune cell type within stroma-rich regions. *FDR < 0.05 by 1-way ANOVA followed by post test in comparison to surgery-alone patients.

reference to it in PDAC. One study by Chmielecki et al. did find that SND1 is somewhat frequently fused with BRAF [inv(7)(q13:q34)], leading to increased MAPK activity in pancreatic acinar carcinoma, but it is not clear that the DNA-binding activity of SND1 was relevant to the oncogenic activity of this fusion (18). Additional work is needed to determine if the activity of these transcription factors is in fact enhanced within the tumor microenvironment following neoadjuvant therapy; in what cell type(s), if any, the activity of these transcription factors is altered; and what the consequences of the apparent increase in RUNX1 and SND1 activity following neoadjuvant therapy are.

It is readily apparent from these data, particularly when comparing transcript levels among the 4 groups of patients, that the addition of radiotherapy to the chemotherapy regimen induced much more profound

changes in gene expression than did chemotherapy alone. While it is not possible to determine from these data, it is interesting to speculate whether radiotherapy (of either modality) alone would induce similar differences in immunologically relevant gene expression as those observed when radiotherapy is combined with chemotherapy. Meanwhile, it is apparent from analysis of spatially resolved differences in protein expression that FOLFIRINOX alone and F + SBRT sometimes had opposing effects. Notably, when looking in immune-rich regions, discrepant data were evident for CD45RO and CD8. When considering these data, it is important to remember that the protein-level data sampled discrete regions within the tumor section, whereas the RNA-level data are drawn from the entire tumor section.

The distinct modality of radiotherapy did not markedly affect the immune phenotype of a PDAC tumor. For instance, no DEGs were identified when comparing F + SBRT– to F + XRT–treated tumors. Additionally, whereas unsupervised hierarchical clustering grouped surgery-alone samples together and FOLFIRINOX-treated samples together, F + SBRT– and F + XRT–treated samples were not distinguished from each other by this algorithm. However, since the dose of radiation delivered to nontumor regions may differ between these treatment modalities, the systemic effects or effects within metastatic sites may in fact differ. Future study is therefore necessary to answer this question in a more definitive manner.

Exposure of tumors to FOLFIRINOX with SBRT was associated with prominent alterations in immune cell markers. For example, FOLFIRINOX plus radiotherapy was linked with significantly lower expression of T cell markers within immune-rich regions of tumors. However, FOLFIRINOX-treated tumors were not denuded of infiltrating immune cells — particularly T cells, based on expression of CD3, CD4, and CD8 — as assessed at surgical resection (occurring on average 6.6 weeks following the end of FOLFIRINOX neoadjuvant therapy). These data with F + SBRT suggest two possible scenarios: (a) F + SBRT leads to $CD8^+$ T cell death within immune- and stroma-rich regions while FOLFIRINOX does not; alternatively, (b) both treatments may result in $CD8^+$ T cell death within these regions, but in FOLFIRINOX-treated patients, new $CD8^+$ T cells are able to infiltrate these regions during the delay between the end of neoadjuvant therapy and surgery, while this process is strongly impaired in F + SBRT–treated tumors. Further studies will be necessary to determine which of these interpretations is more likely. In addition to changes in T cell markers, other notable expression differences were evident. For example, expression of B cell markers (CD19, CD20) was also significantly lower in immune-rich regions of tumors upon exposure to FOLFIRINOX with or without SBRT. The ability of chemotherapy and radiotherapy to modulate B cell populations may be of interest in light of data indicating that B cells are a key component of the PDAC tumor microenvironment (19–22). Immune checkpoint molecules were also differentially expressed based on exposure to F + SBRT. In CD45-rich areas, FOLFIRINOX treatment was associated with greater PD-L1, while in immune-rich and stroma-rich regions, F + SBRT was associated with significantly lower PD-1. These data present a scenario whereby subsequent exposure to conventional therapy might prime the host to PD-1/PD-L1–targeted therapy. Finally, there was a statistically significant downregulation of VISTA by exposure to F + SBRT in all 3 regions (tumor-, immune cell–, or stroma-rich regions). This consistent pattern in VISTA contrasts that for other immune checkpoint molecules that were not appreciably altered. Considering the downregulation of biomarkers related to T cells and immune checkpoints, it emphasizes the need for identifying other therapeutic modalities (i.e., vaccines, TLR agonists) that might act to increase the number and quality of infiltrating T cells into PDAC tumors (23–25).

There are some caveats and limits to this study that we must acknowledge. First, as noted in Table 1, there was a delay of several weeks between the end of neoadjuvant therapy and surgical resection. Thus, the immediate effects of FOLFIRINOX and/or radiotherapy are likely diluted due to this time delay. At the same time, this time delay also indicates that the effects observed here are durable and may indicate a long-term "reprogramming" of the tumor microenvironment. Second, this study was not powered to detect relationships between differences in the expression of these genes and patient outcome. Moreover, this was a retrospective rather than prospective study. Finally, we must note that patients who received neoadjuvant therapy tended to have more advanced disease. All patients who received upfront resection were classified as having "resectable" disease at baseline. In contrast, 5 of the 6 FOLFIRINOX-treated patients and all of the F + SBRT–treated patients were classified as having "borderline resectable" disease. Similarly, 4 of the 6 F + XRT–treated patients had borderline resectable disease while the remaining 2 had locally advanced disease initially. Only patients who eventually had surgical resection were included in this study.

Taken together, these results identify gene expression profiles within the tumor microenvironment associated with exposure to neoadjuvant therapy and provide preliminary evidence on biomarkers that may influence the suitability of chemotherapy and radiotherapy to be combined with other immune-based

treatment strategies. Overall, these results provide insight into how the conventional therapies modulate tumor, immune, and stromal components of the PDAC tumor microenvironment.

Methods

Patient selection. Tumor specimens from 24 patients were retrospectively selected from those who had undergone pancreatectomy or Whipple surgery at Emory University (Table 1). All patients had surgery between 2011 and 2016 and had archival formalin-fixed, paraffin-preserved (FFPE) tumor tissue available for research. Patient tumors were stratified into 4 distinct groups based on modality of neoadjuvant treatment. Patients for each group (n = 6 per group) were matched to the best of our ability on the basis of lymphovascular invasion and perineural invasion. Patients were not matched on the basis of sex, race, or age.

RNA isolation and nCounter NanoString gene expression profiling. RNA was isolated from FFPE sections of patient tumors by the Emory Integrated Genomics Core (EIGC). Briefly, for each patient, four 5-micron FFPE sections were scraped into 1.5-ml Eppendorf tubes. RNA was extracted with the EZ FFPE RNA kit (Omega BioTek). RNA was eluted in 30 μl nuclease-free water. RNA quality and quantity were determined using a Nanodrop 1000 (Thermo Fisher) and 6000 RNA Nano assay (Agilent). RNA input was scaled based on DV 300 value to 50 ng (50 ng/DV300 × 100) and processed according to the nCounter XT Assay User Manual (NanoString Inc., MAN-10023-11). The EIGC carried out gene expression profiling using the Pan-Cancer Immune Profiling Panel (NanoString Inc.) as previously described (26). This panel analyzes gene expression from n = 730 genes involved in the immune response. Briefly, scaled RNA was hybridized with biotin-labeled capture probes and fluorescently labeled reporter probes for 18 hours at 65°C. Following hybridization, samples were injected into a NanoString SPRINT cartridge and loaded onto the SPRINT instrument where excess capture probe and reporter probe were removed, and hybridized mRNAs were immobilized for imaging. Following image acquisition, mRNA counts were extracted from raw RCC files using nSolver analysis software v3.0 (NanoString Inc.) and exported as.csv files for further analysis.

Spatially resolved, multiplexed histologic analysis of protein expression levels. Spatially resolved quantitation of the expression levels of 27 immunologically relevant proteins (plus 2 normalization controls and 2 negative controls) was measured using the GeoMX platform (NanoString Inc.), as previously described (27, 28). Briefly, glass slides containing 5-μm FFPE sections of archival surgically resected patient PDAC tumors were stained with a cocktail of 31 oligonucleotide-tagged antibodies: 27 directed against immunologically relevant proteins of interest, 2 directed against normalization/control proteins, and 2 isotype controls (Supplemental Table 1). The oligonucleotide tags were specific for each type of antibody and were conjugated to the antibodies by way of an UV-cleavable linker. Each selected primary antibody was coupled to a unique 70-nt indexing oligo (NanoString Inc., custom conjugation service). After conjugation, antibody:oligo conjugates were subjected to HPLC to purify these conjugated products from any remaining unconjugated antibodies free of their oligo tag. Slides were also stained with fluorescently labeled antibodies directed against αSMA, CD45, and pan-cytokeratin, which served as visualization markers. Slides were imaged on the GeoMX platform, which functions in part as a fluorescent slide scanner. Regions of interest (ROIs; n = 12/slide) were selected on the basis of the visualization markers, using a custom-designed web-based control program (NanoString Inc.). Criteria used to select ROIs are described in the Results. After ROIs were selected, the GeoMX platform used an automatically controlled UV laser to illuminate each ROI in turn, specifically cleaving oligonucleotide tags within the ROI but not in surrounding tissue. A microcapillary collection system collected the liberated oligonucleotides from each region and plated them into an individual well on a microtiter plate. This process was repeated in turn for each ROI. After ROI collection was complete, oligonucleotides were hybridized to complimentary NanoString counting beads and counted using an nCounter analysis platform (NanoString Inc.). A highly detailed description of the GeoMX platform and related staining and imaging procedures is contained in a recent report by Amaria et al. (27).

Availability of data and material. Data from the NanoString gene (mRNA) expression profiles have been submitted to the Gene Expression Omnibus database (29) and is available under accession GSE129492.

Statistics. Normalization and differential expression analysis of NanoString nCounter (RNA) data were performed by using default settings on nSolver 4.0 Analysis Software. Pairwise differential expression was conducted by using nSolver, which performed a 2-tailed t test on the log-transformed normalized data. Genes were considered significantly differentially expressed between 2 groups if the FDR was less than 0.05.

All statistical tests for protein-based analyses were conducted using 1-way ANOVA followed by Bonferroni post hoc test (GraphPad Prism). One-way ANOVA P values were adjusted for multiple comparisons

using the FDR. Differences between the control (surgery-alone) group and experimental groups were considered statistically significant when FDR < 0.05 and post test results were $P < 0.05$.

Gene set enrichment overlaps were computed using the Molecular Signatures Database v6.2 maintained by the Broad Institute (30, 31). Protein-protein interaction enrichment analysis and the MCODE algorithm were carried out using the online analysis tools maintained by Metascape.org (32). Transcription factor–binding motif overlap and enrichment was calculated using the TRANSFAC and JASPAR PWMs databases and online tools maintained by EnrichR (http://amp.pharm.mssm.edu/Enrichr/#) (9–11).

Study approval. Ethical approval for this study was granted by the Emory University Institutional Review Board (protocol IRB00094907).

Author contributions

MRF, LS, WS, and GBL conceived this work and participated in experimental design. LS, AK, MZ, and WS reviewed clinical records to select archival specimens to include in this study and obtained specimens from pathology. MRF and HC analyzed RNA expression profiles. MRF, MBW, JG, YL, and GBL analyzed and acquired spatially resolved protein expression data. MRF, MBW, HC, MZ, JMS, DK, PP, WS, and GBL worked together on the interpretation of data. MRF and HC carried out statistical tests. MRF, MBW, SKM, BE, WS, and GBL took primary roles in the drafting and revisions of manuscript. All authors edited and provided feedback on the manuscript. All authors have read and approved of this final manuscript.

Acknowledgments

This work was funded in part by in-kind grant support (materials and lab services) from NanoString Inc. as well as research funds from the Hirshberg Foundation and NIH grants R01 CA208253 and R01228406. We would like to acknowledge the contribution of the EIGC, which is subsidized by the Emory University School of Medicine and is one of the Emory Integrated Core Facilities. Research reported in this publication was supported in part by the EIGC Shared Resource and the Biostatistics and Bioinformatics Shared Resource of Winship Cancer Institute of Emory University and NIH/National Cancer Institute under award P30CA138292. The content is solely the responsibility of the authors and does not necessarily represent the official views of the NIH.

Address correspondence to: Walid Shaib or Gregory B. Lesinski, Department of Hematology and Medical Oncology, Winship Cancer Institute of Emory University, 1365 Clifton Road NE, Atlanta, Georgia 30322, USA. Phone: 404.778.1900; Email: walid.shaib@emory.edu (WS). Phone: 404.778.3072; Email: gregory.b.lesinski@emory.edu (GBL).

MRF's current address is: Q2 Solutions, Marietta, Georgia, USA.

1. Siegel RL, Miller KD, Jemal A. Cancer statistics, 2019. *CA Cancer J Clin*. 2019;69(1):7–34.
2. Rahib L, Smith BD, Aizenberg R, Rosenzweig AB, Fleshman JM, Matrisian LM. Projecting cancer incidence and deaths to 2030: the unexpected burden of thyroid, liver, and pancreas cancers in the United States. *Cancer Res*. 2014;74(11):2913–2921.
3. Raufi AG, Manji GA, Chabot JA, Bates SE. Neoadjuvant treatment for pancreatic cancer. *Semin Oncol*. 2019;46(1):19–27.
4. D'Angelo F, et al. Neoadjuvant treatment in pancreatic cancer: Evidence-based medicine? A systematic review and meta-analysis. *Med Oncol*. 2017;34(5):85.
5. Uzunparmak B, Sahin IH. Pancreatic cancer microenvironment: a current dilemma. *Clin Transl Med*. 2019;8(1):2.
6. Ducreux M, et al. Systemic treatment of pancreatic cancer revisited. *Semin Oncol*. 2019;46(1):28–38.
7. Mace TA, et al. Pancreatic cancer-associated stellate cells promote differentiation of myeloid-derived suppressor cells in a STAT3-dependent manner. *Cancer Res*. 2013;73(10):3007–3018.
8. Schumacher TN, Schreiber RD. Neoantigens in cancer immunotherapy. *Science*. 2015;348(6230):69–74.
9. Khan A, et al. JASPAR 2018: update of the open-access database of transcription factor binding profiles and its web framework. *Nucleic Acids Res*. 2018;46(D1):D260–D266.
10. Chen EY, et al. Enrichr: interactive and collaborative HTML5 gene list enrichment analysis tool. *BMC Bioinformatics*. 2013;14:128.
11. Kuleshov MV, et al. Enrichr: a comprehensive gene set enrichment analysis web server 2016 update. *Nucleic Acids Res*. 2016;44(W1):W90–W97.
12. Topham DJ, Reilly EC. Tissue-resident memory $CD8^+$ T cells: From phenotype to function. *Front Immunol*. 2018;9:515.
13. Chen C, Zhao S, Karnad A, Freeman JW. The biology and role of CD44 in cancer progression: therapeutic implications. *J Hematol Oncol*. 2018;11(1):64.
14. ElTanbouly MA, Croteau W, Noelle RJ, Lines JL. VISTA: a novel immunotherapy target for normalizing innate and adaptive

immunity. *Semin Immunol*. 2019;42:101308.
15. Hong D, et al. RUNX1-dependent mechanisms in biological control and dysregulation in cancer. *J Cell Physiol*. 2019;234(6):8597–8609.
16. Cheng Y, et al. RUNX1 promote invasiveness in pancreatic ductal adenocarcinoma through regulating miR-93. *Oncotarget*. 2017;8(59):99567–99579.
17. Ochoa B, Chico Y, Martínez MJ. Insights into *SND1* oncogene promoter regulation. *Front Oncol*. 2018;8:606.
18. Chmielecki J, et al. Comprehensive genomic profiling of pancreatic acinar cell carcinomas identifies recurrent RAF fusions and frequent inactivation of DNA repair genes. *Cancer Discov*. 2014;4(12):1398–1405.
19. Pylayeva-Gupta Y, et al. IL35-Producing B cells promote the development of pancreatic neoplasia. *Cancer Discov*. 2016;6(3):247–255.
20. Lee KE, et al. Hif1a deletion reveals pro-neoplastic function of B cells in pancreatic neoplasia. *Cancer Discov*. 2016;6(3):256–269.
21. Gunderson AJ, et al. Bruton tyrosine kinase-dependent immune cell cross-talk drives pancreas cancer. *Cancer Discov*. 2016;6(3):270–285.
22. Zhao Y, et al. Regulatory B cells induced by pancreatic cancer cell-derived interleukin-18 promote immune tolerance via the PD-1/PD-L1 pathway. *Oncotarget*. 2018;9(19):14803–14814.
23. Omar HA, Tolba MF. Tackling molecular targets beyond PD-1/PD-L1: Novel approaches to boost patients' response to cancer immunotherapy. *Crit Rev Oncol Hematol*. 2019;135:21–29.
24. Osipov A, Zaidi N, Laheru DA. Dual checkpoint inhibition in pancreatic cancer: revealing the limitations of synergy and the potential of novel combinations [published online ahead of print July 18, 2019]. *JAMA Oncol*. doi: 10.1001/jamaoncol.2019.1583.
25. Wu AA, Jaffee E, Lee V. Current status of immunotherapies for treating pancreatic cancer. *Curr Oncol Rep*. 2019;21(7):60.
26. Mace TA, et al. IL-6 and PD-L1 antibody blockade combination therapy reduces tumour progression in murine models of pancreatic cancer. *Gut*. 2018;67(2):320–332.
27. Amaria RN, et al. Neoadjuvant immune checkpoint blockade in high-risk resectable melanoma. *Nat Med*. 2018;24(11):1649–1654.
28. Blank CU, et al. Neoadjuvant versus adjuvant ipilimumab plus nivolumab in macroscopic stage III melanoma. *Nat Med*. 2018;24(11):1655–1661.
29. Subramanian A, et al. Gene set enrichment analysis: a knowledge-based approach for interpreting genome-wide expression profiles. *Proc Natl Acad Sci USA*. 2005;102(43):15545–15550.
30. Liberzon A, Subramanian A, Pinchback R, Thorvaldsdóttir H, Tamayo P, Mesirov JP. Molecular signatures database (MSigDB) 3.0. *Bioinformatics*. 2011;27(12):1739–1740.
31. Tripathi S, et al. Meta- and Orthogonal Integration of Influenza "OMICs" Data Defines a Role for UBR4 in Virus Budding. *Cell Host Microbe*. 2015;18(6):723–735.
32. Clough E, Barrett T. The Gene Expression Omnibus Database. *Methods Mol Biol*. 2016;1418:93–110.